Technical Note

Lateral Responses of a Model Pile in Biocemented Sand

Yang Xiao, M.ASCE[1]; Armin W. Stuedlein, M.ASCE[2]; Xiang He, S.M.ASCE[3]; Fei Han, A.M.ASCE[4]; T. Matthew Evans, M.ASCE[5]; Zhengyu Pan[6]; Hai Lin[7]; Jian Chu, M.ASCE[8]; and Leon van Paassen[9]

Abstract: This technical note aims to investigate the effects of biotreatment on the response of a concrete model pile embedded in poorly graded sand through lateral loading tests. The bending moment profiles along pile length were obtained from strain gauges collected during the pile load tests. The pile deflection and soil resistance were derived from a bending moment profile based on beam theory. The ultimate lateral resistance of the pile with biotreatment was 2.6 times as large as that without biotreatment. The bending moment for the pile in biotreated soil is significantly smaller than that for the pile in untreated soil due to the reduction in curvature. The spatial distribution of calcium carbonate generated during the biotreatment was obtained from 1,800 sand samples, which was also validated by the scanning electron microscope images. Biotreatment of sand surrounding a pile is demonstrated to be a promising measure to effectively improve the lateral capacity of the pile. **DOI: 10.1061/(ASCE)GM.1943-5622.0002179**. © *2021 American Society of Civil Engineers*.

Introduction

The lateral resistance of a pile is controlled by the confining condition and the stiffness of the surrounding soil near the ground surface (Meyerhof et al. 1981; Randolph 1981; Han et al. 2017). When the lateral load applied on a pile exceeds its lateral capacity, the pile undergoes excessive displacement and rotation, leading to damage or failure of the superstructure above it (Knappett and Madabhushi 2009). There are generally two categories of methods that can be used to increase the lateral capacity of a pile: (1) changing the type or geometry of the pile, and (2) improving the strength or stiffness of the surrounding soil. Various modifications to deep foundations have proven to be effective to improve lateral capacity: use of steel casing with drilled shafts (Li et al. 2019) and adding bearing plates or wings to piles (Bienen et al. 2012; Stone et al. 2018). Ground improvement methods that have been used to strengthen the soil surrounding the pile include compacted granular fill (Rollins et al. 2010b), soil mixing and jet grouting (Rollins et al. 2010a; Faro et al. 2015), and cement grouting (Yu et al. 2018). The binding agents used in the latter methods are mainly cement and chemical grout, which may be difficult to construct due to the grout viscosity and use of heavier machinery (e.g., deep mixing system and grout plants), although these agents could improve soil properties (Kang et al. 2016; Rahimi et al. 2016). As an emerging technique in geotechnical engineering, biogrouting takes advantages of the natural biogeochemical process, presenting advantages over the traditional grouting methods that employ synthetic materials (Achal et al. 2015). Promising results have shown that the biogrouting technique through a microbially induced calcium carbonate precipitation (MICP) process for ground improvement (Whiffin et al. 2007; van Paassen et al. 2010; DeJong et al. 2013; San Pablo et al. 2020) is effective due to the enhancement in the strength and stiffness of soil (van Paassen et al. 2010; Montoya and DeJong 2015; Yang et al. 2017; Xiao et al. 2019c; Yang et al. 2019; Nafisi et al. 2020; Kashizadeh et al. 2021).

Recently, biogrouting has been utilized to enhance the shaft resistance of pervious concrete piles subjected to axial loads in compression (Lin et al. 2016) and in tension (Lin et al. 2018). The mechanisms of this improvement involve the formation of MICP-improved soil along the shaft of the pile. Xiao et al. (2020b) developed a biogrouting technique to increase the toe resistance of precast concrete piles by injecting biogrouting solutions near the pile toe through a silicon tube embedded in the pile center. Although these studies have shown the effectiveness of biogrouting in the improvement of pile performance under axial loads, no attempt has been made to assess the performance of laterally loaded piles in soil strengthened by biogrouting. The main objective of this technical note is to evaluate the effectiveness of MICP-based biogrout to improve lateral capacity of piles. The lateral load corresponding to a lateral pile head deflection of $0.1D$, with D being the pile diameter, is defined as the ultimate resistance for the interpretation of the test results (Chen et al. 2011; Nasr 2014). Instrumented model pile tests were performed to compare the pile response with lateral loads in soil both with and without

[1]Professor, Key Laboratory of New Technology for Construction of Cities in Mountain Area, State Key Laboratory of Coal Mine Disaster Dynamics and Control, School of Civil Engineering, Chongqing Univ., Chongqing 400045, China. ORCID: https://orcid.org/0000-0002-9411-4660. Email: hhuxyanson@163.com

[2]Professor, School of Civil and Construction Engineering, Oregon State Univ., Corvallis, OR 97331 (corresponding author). ORCID: https://orcid.org/0000-0002-6265-9906. Email: armin.stuedlein@oregonstate.edu

[3]Ph.D. Candidate, School of Civil Engineering, Chongqing Univ., Chongqing 400045, China. Email: medihe@163.com

[4]Postdoctoral Associate, Lyles School of Civil Engineering, Purdue Univ., West Lafayette, IN 47907, China. ORCID: https://orcid.org/0000-0001-7492-2778. Email: hanfei@purdue.edu

[5]Professor, School of Civil and Construction Engineering, Oregon State Univ., Corvallis, OR 97331. ORCID: https://orcid.org/0000-0002-8457-7602. Email: matt.evans@oregonstate.edu

[6]Graduate Student, School of Civil Engineering, Chongqing Univ., Chongqing 400045, China. Email: zhengyupanmicp@cqu.edu.cn

[7]Assistant Professor, Dept. of Civil and Environmental Engineering, Louisiana State Univ., Baton Rouge, LA 70803. ORCID: https://orcid.org/0000-0002-1641-4588. Email: hailin1@lsu.edu

[8]Professor, School of Civil and Environmental Engineering, Nanyang Technological Univ., 10 Blk N1, 50 Nanyang Ave., Singapore 639798. Email: cjchu@ntu.edu.sg

[9]Associate Professor, Center for Bio-mediated and Bio-inspired Geotechnics, Arizona State Univ., Tempe, AZ 85287-3005. Email: leon.vanpaassen@asu.edu

Note. This manuscript was submitted on February 14, 2021; approved on June 26, 2021; published online on August 26, 2021. Discussion period open until January 26, 2022; separate discussions must be submitted for individual papers. This technical note is part of the ***International Journal of Geomechanics***, © ASCE, ISSN 1532-3641.

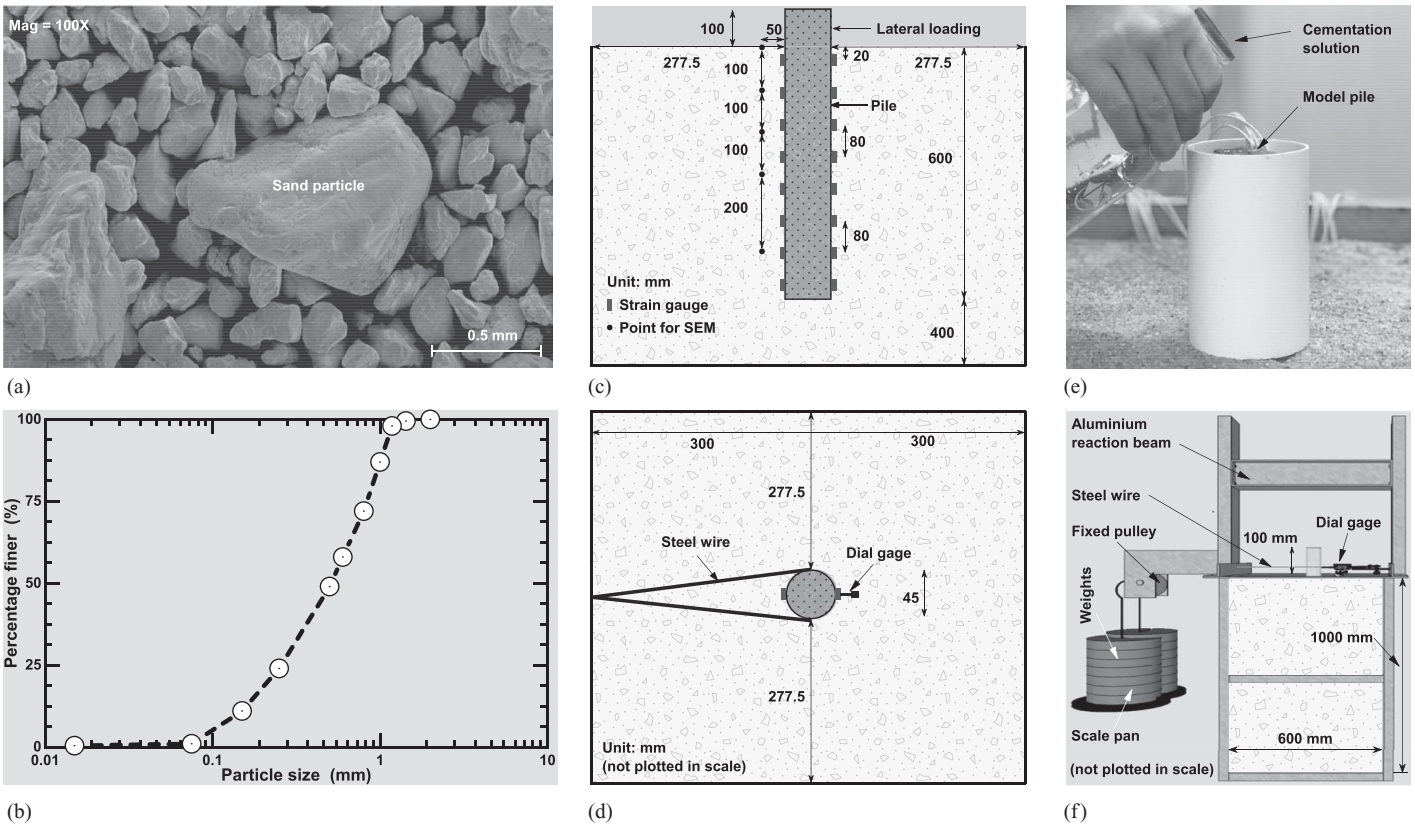

Fig. 1. (a) SEM image of the tested sands with the magnification of 100; (b) particle size distribution curve; (c) side view of the lateral loading test; (d) top view of the lateral loading test; (e) image of adding solutions; and (f) schematic of the test model.

Table 1. Physical properties of the silica sand used in the tests

Characteristic	Symbol	Values
Mean particle size (mm)	D_{50}	0.51
Coefficient of uniformity	C_u	4.4
Specific gravity	G_s	2.69
Maximum void ratio	e_{max}	0.79
Minimum void ratio	e_{min}	0.39

biogrouting. Comparisons were made in terms of the loading–displacement curves and bending moment profiles. The spatial distribution of calcium carbonate in the sand surrounding the pile was quantitatively evaluated and the microstructure of the biocemented sand was analyzed by a scanning electron microscope (SEM).

Materials and Methods

Characteristics of Sand and Model Pile

The test sand is a silica sand that was obtained from the Luyangpu River, Fujian Province, China. Fig. 1(a) shows the SEM images of the sand particles with angular to subangular shapes. Fig. 1(b) shows the particle size distribution of the test sand. The physical properties of the soil are summarized in Table 1. According to the Unified Soil Classification System (ASTM D2487-06, ASTM 2006), the sand is classified as poorly graded. The solid circular concrete pile used in this study is 45 mm in diameter and 700 mm in length. Sixteen strain gauges were installed symmetrically on the two sides of the pile. As shown in Fig. 1(c), the strain gauges were installed at a spacing of 80 mm along the pile length. All strain gauges were coated with epoxy to be protected from damage. The sampling frequency for the strain gauges was 20 Hz in the lateral loading tests.

Bacteria and Cementation Solution Preparation

A urease-producing bacteria strain *Sporosarcina pasteurii* [American Type Culture Collection (ATCC) 11859] was used for the biocementation process. The bacteria was cultured in a liquid medium, which consists of 20 g/L yeast extract, 12 mg/L $MnCl_2 \cdot H_2O$, 10 g/L NH_4Cl, and 24 mg/L $NiCl_2 \cdot 6H_2O$ with a pH of 9.0 (Liu et al. 2019; Xiao et al. 2019a). The bacteria cultivation and preservation procedures used in this study are same as those introduced by Xiao et al. (2019b). The urease activity was approximately 2 mM urea/min. The cementation solution is composed of equal mole concentration of $CaCl_2$ and urea (0.5 mol/L).

Sample Preparation and Biotreatment

The model pile tests were performed in a square cuboid chamber with a width of 600 mm and a height of 1,000 mm. The chamber was reinforced by aluminum beams along the edges. The sand sample was prepared with the test pile fixed in the chamber to simulate the case of a wished-in-place nondisplacement pile. The sample preparation was performed in 20 lifts by air pluviation, and the relative density of the prepared sand sample was 68%. As shown in Figs. 1(c and d), the 45-mm-diameter circular concrete pile was embedded 600 mm in the test sand, and the distance from the pile toe to the chamber bottom was 400 mm. Two model pile tests were carried out to assess the effectiveness of biocementation in improving the lateral pile capacity. For *Test I* (with biogrouting), the biogrouting

process started with the injection of 1 L of bacteria solution around the pile. A 110-mm-long PVC pipe with an inner diameter (50 mm) slightly greater than the diameter of the pile [as shown in Fig. 1(e)] was used to guide the flow of the solution. The bacteria are distributed to the sand around the pile through gravity percolation (Mahawish et al. 2019; Xiao et al. 2019b). After a retention of 2 h after the injection of the bacteria solution, 3 L of the cementation solution was then introduced to the sand. The sand was then cured for 10 h to allow the calcium carbonate precipitation and cementation among sand particles. This two-step procedure of injecting bacteria and cementation solution was repeated six times to maximize the strength of the biocementation. For *Test II* (a control test without biogrouting), the bacteria solution was replaced with deionized water, all else being the same as *Test I*. The saturation of sand sample was around 15% after the injections of solutions for both tests.

Lateral Loading Procedure

The two lateral pile loading tests were performed in accordance with the standard loading procedure outlined in the standard [ASTM D3966/D3966M-07(2013)e1, ASTM 2013]. The lateral load was applied using a pulley system, which consisted of a fixed pulley mounted on the edge of the test chamber, adjustable weights, and a set of steel wires connecting to the weights and the loading points at the pile head on their two ends, as shown in Fig. 1(f). The loading points on the pile were located 2 mm above the sand surface. A dial gauge was placed between the pile and an aluminum reaction beam to measure the lateral displacement of the pile head.

Quantification of Precipitated Calcium Carbonate

After the pile loading tests, cemented sand samples were collected at depth intervals of 0.4 m as the sand was gently removed from the chamber layer by layer. A total of 1,800 sand samples (each weighing about 20–30 g) were obtained at different locations with respect to the pile at 15 depths, producing a spatial distribution of the calcium carbonate ($CaCO_3$) precipitated in the chamber. Those samples were flushed with deionized water to remove residual chemicals and then oven-dried at 60°C for 4 days. The $CaCO_3$ content was measured using an acid washing method (Al Qabany et al. 2012; Feng and Montoya 2016; Xiao et al. 2020a; Ma et al. 2021). Each sample was washed using an aqueous hydrochloric acid (1 mol/L) solution. After the $CaCO_3$ precipitates were completely dissolved, the sample was rinsed with deionized water for a minimum of 10 times to remove the dissolved salts. The sample was then oven-dried at 105°C for 24 h after washing. The difference in the masses of the oven-dried sample before and after the acid washing is the weight of $CaCO_3$ in the sample.

Microstructure Analysis

SEM images were taken to investigate the microstructures of sand samples before and after biogrouting. Prior to the SEM, the untreated sand sample and the sand samples collected near the pile–sand interface were rinsed with distilled water, dried at 60°C for 24 h, and then coated with gold under vacuum. A Thermo Fisher Quattro SEM instrument (Waltham, MA) was used to capture the microstructures.

Experimental Results and Discussion

Load–Displacement and Bending Moment Responses

Fig. 2(a) compares the relationships between the lateral load and displacement at the pile head obtained from *Test I* (with biogrouting) and *Test II* (without biogrouting). The load–displacement curve for the pile in the biotreated soil is significantly stiffer than that in the untreated soil. Using a commonly accepted definition of the ultimate lateral resistance of a pile as the load corresponding to a lateral displacement of 0.1*D*, with *D* being the pile diameter (Nasr 2014), the ultimate lateral resistance for the pile in the

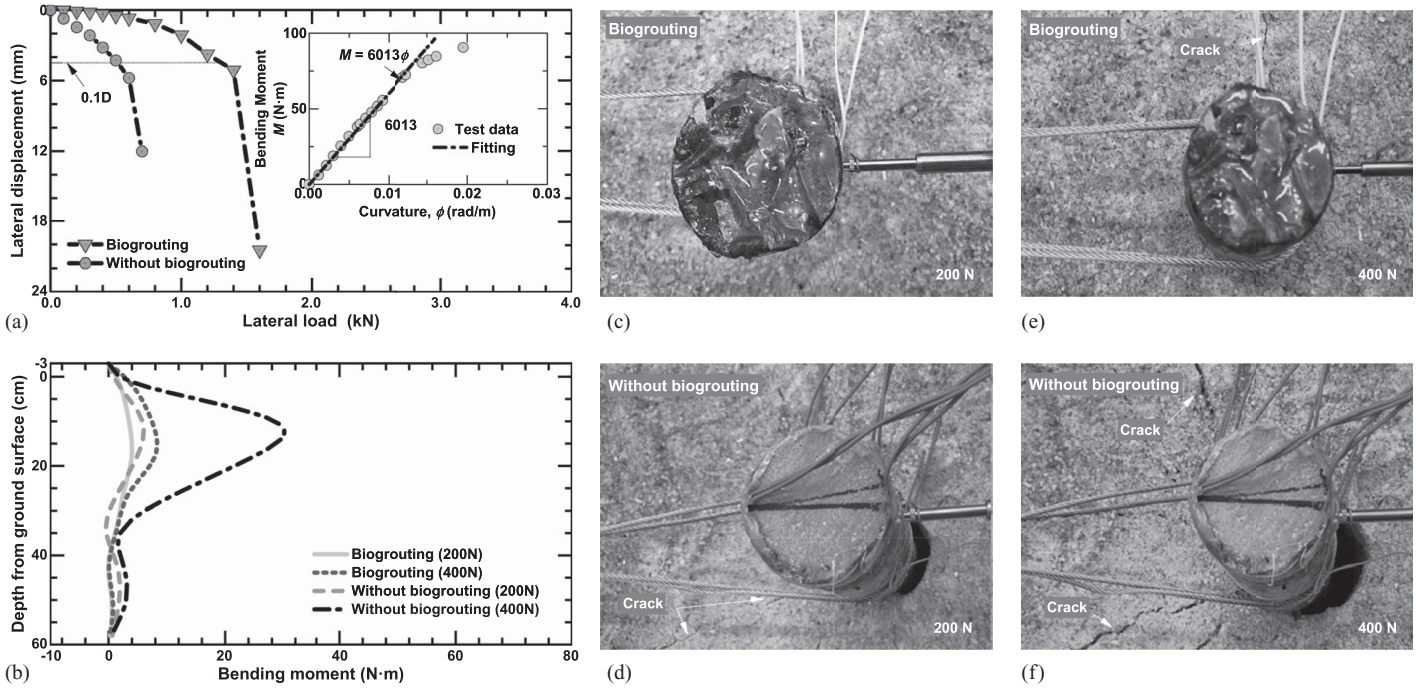

Fig. 2. Lateral responses of piles: (a) lateral load versus lateral displacement; (b) comparisons of bending moment; (c and d) responses of pile in sand with and without biogrouting at a lateral load of 200 N; and (e and f) responses of pile in sand with and without biogrouting at a lateral load of 400 N.

Int. J. Geomech., 2021, 21(11): 06021027

biotreated soil was 1.31 kN, which was approximately 2.6 times larger than the untreated soil (0.5 kN). The load–displacement responses for both piles were highly nonlinear: the lateral load increased at a degrading rate with increasing lateral displacement, and a significant lateral displacement was observed soon after the ultimate load level when the pile–head displacement reached $0.1D$.

The bending moment M in pile at depth z was calculated from the strain gauge data by

$$M(z) = EI\phi(z) = \frac{EI\Delta\varepsilon(z)}{D} \tag{1}$$

where E = Young's modulus of the pile; I = area moment of inertia of pile cross section; $\phi(z)$ and $\Delta\varepsilon(z)$ = pile curvature and the difference between the tensile and compressive strains at depth z, respectively. The moment–curvature (M–ϕ) relationship [see the inset of Fig. 2(a)] for the circular concrete piles was obtained by performing a three-point bending test using a sampling frequency of 20 Hz for the strain gauges following procedures prescribed in ASTM C293/C293M-16 (ASTM 2016). The curing time for the concrete pile in the three-point bending test was 14 days, which is the same as that for the model piles used in the loading tests. The bending moment M increases linearly with increasing pile curvature ϕ until a bending moment of 75 N · m is reached. The Young's modulus of the concrete was estimated to be 29.9 GPa. Fig. 2(b) compares the profiles of the bending moment along the pile length in the biotreated and untreated sands at the applied loads of 200 and 400 N, respectively. For both cases, the bending moment initially increases with depth to a peak value and then decreases, reaching

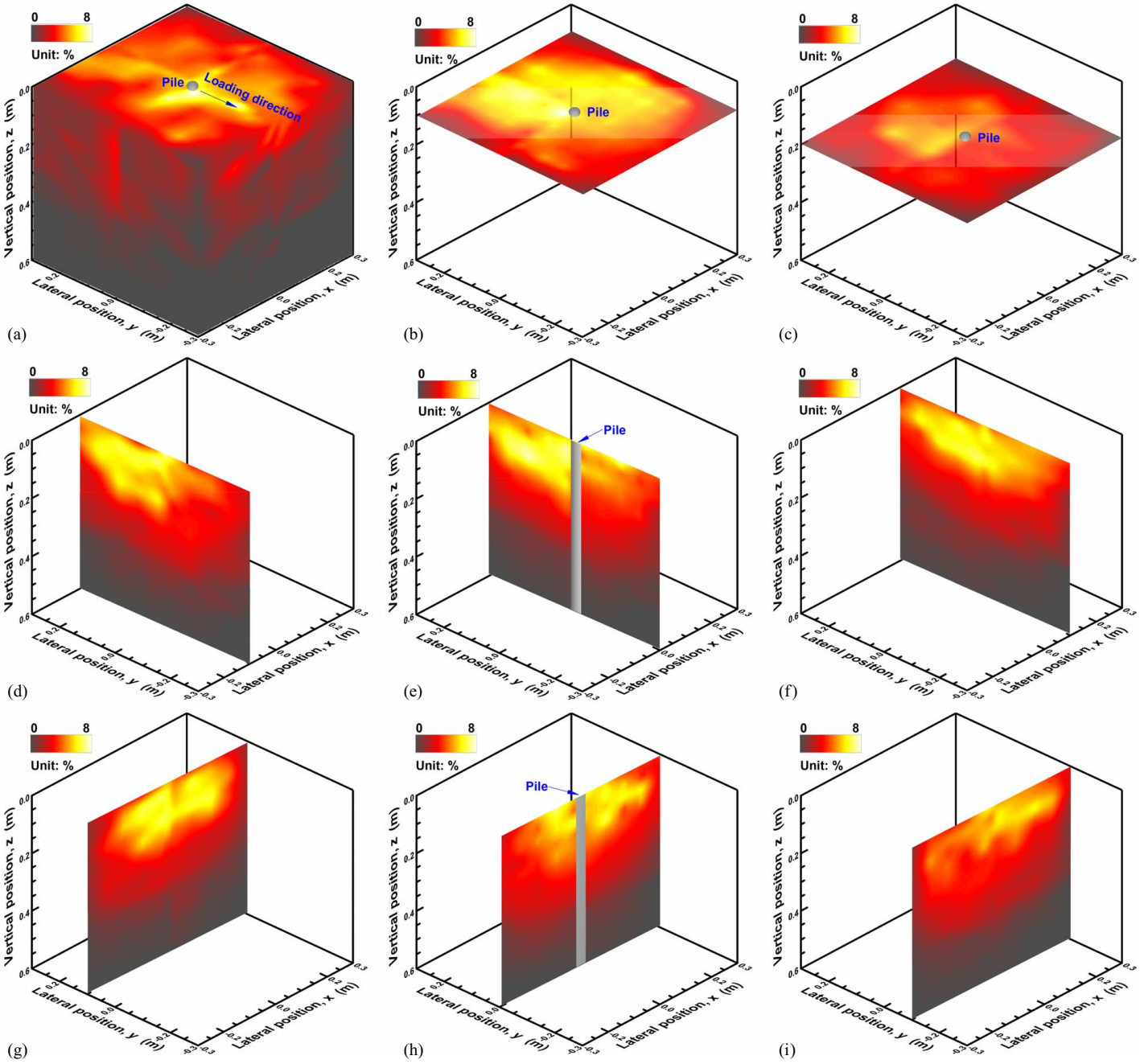

Fig. 3. Distribution of calcium carbonate in the biotreated sand for the model pile: (a) overview of the calcium carbonate distribution; and at the slices of (b) $z = 0.1$ m; (c) $z = 0.2$ m; (d) $x = -0.1$ m; (e) $x = 0$ m; (f) $x = 0.1$ m; (g) $y = 0.1$ m; (h) $y = 0$ m; and (i) $y = -0.1$ m.

Int. J. Geomech., 2021, 21(11): 06021027

nearly zero close to the base of the pile. The maximum bending moment was 30 N · m for *Test II (untreated sand)*, which was 3.2 times greater (9.3 N · m) than that for *Test I (biocemented sand)* at an applied load of 400 N. The maximum bending moment in the pile was found at a slightly greater depth in the biotreated sand than in the untreated sand.

Figs. 2(c–f) show the soil surface near the pile in *Tests I* and *II*, respectively, taken at lateral loads of 200 and 400 N. Cracks at the soil surface started to occur at a lateral load of 200 N and propagated into larger cracks near the pile head with a continuous increase in lateral load. Note that the cracks occurred mostly along directions with small angle with respect to the loading direction in front of the pile in untreated sand, whereas the major cracks were almost perpendicular to the loading direction on the side of the pile in the biotreated sand, similar to responses of cased drilled shafts in medium stiff to stiff plastic soils reported by Li et al. (2019). According to the strain wedge theory (Ashour et al. 1998), the opening fan angle (the angle between the edge of the mobilized soil wedge in front of the pile and the loading direction) is dependent on the internal friction angle of the soil. The greater fan angle observed for the biotreated soil reflects the increased internal friction angle caused by the biocementation process.

Distribution of Calcium Carbonate in Sand

Fig. 3(a) shows the spatial distribution of the $CaCO_3$ content in sand after the load test was performed. Figs. 3(b–i) show the distribution of the $CaCO_3$ content within several selected cross sections of the biocemented sand. The origin of the coordinates in Fig. 3 is positioned at the intersection between the pile axis and the ground surface. Brighter color in the figure represents greater $CaCO_3$ contents. As shown in Figs. 3(b–i), the maximum $CaCO_3$ content was found near a depth of 0.1 m. The effective $CaCO_3$ precipitation was mainly found within the depth of 0.2 m [bright color in Figs. 3(d–i)], whereas the $CaCO_3$ distribution is heterogeneous [Figs. 3(d–f)]. The $CaCO_3$ distribution perpendicular to the loading direction is more symmetrical than in the loading direction. For example, as shown in Fig. 3(e), most of $CaCO_3$ precipitates behind the pile. The star-shaped distribution near the ground surface might have resulted from the formation of preferential flow paths when the solutions were injected through the PVC pipe. However, the $CaCO_3$ distribution becomes more uniform with increasing depth as the biocementation solution evenly spreads in sand when flowing through the sand under gravity. Note that the $CaCO_3$ content in front of the pile along the loading direction (approximately 3%–5%) within the depth of 0.2 m is much lesser than that (around 6%–8%) behind the pile, as shown in Figs. 3(d–f). Had the $CaCO_3$ precipitation in front of the pile been as large as that behind the pile, the lateral pile resistance would have been even greater than that observed in the present study.

Microstructure of Biotreated Sands at the Soil–Pile Interface

Sand samples [50 mm apart from the sand–pile interface, see Fig. 1(c)] were collected to analyze their microstructure after biotreatment. Fig. 4 presents SEM images for the microstructure of the biocemented sands collected at five locations (soil surface, 0.1, 0.2, 0.3, and 0.5 m in depth) behind the pile. It is obvious that the $CaCO_3$ content is larger at the depth of 0.1 m [Fig. 4(b)] than that in other depths, which validates the measured results of the $CaCO_3$ distribution in the former section. The $CaCO_3$ crystals are observed at the surface and contacts of sand particles and in the pore space, as shown in Figs. 4(a–d). The observed precipitation

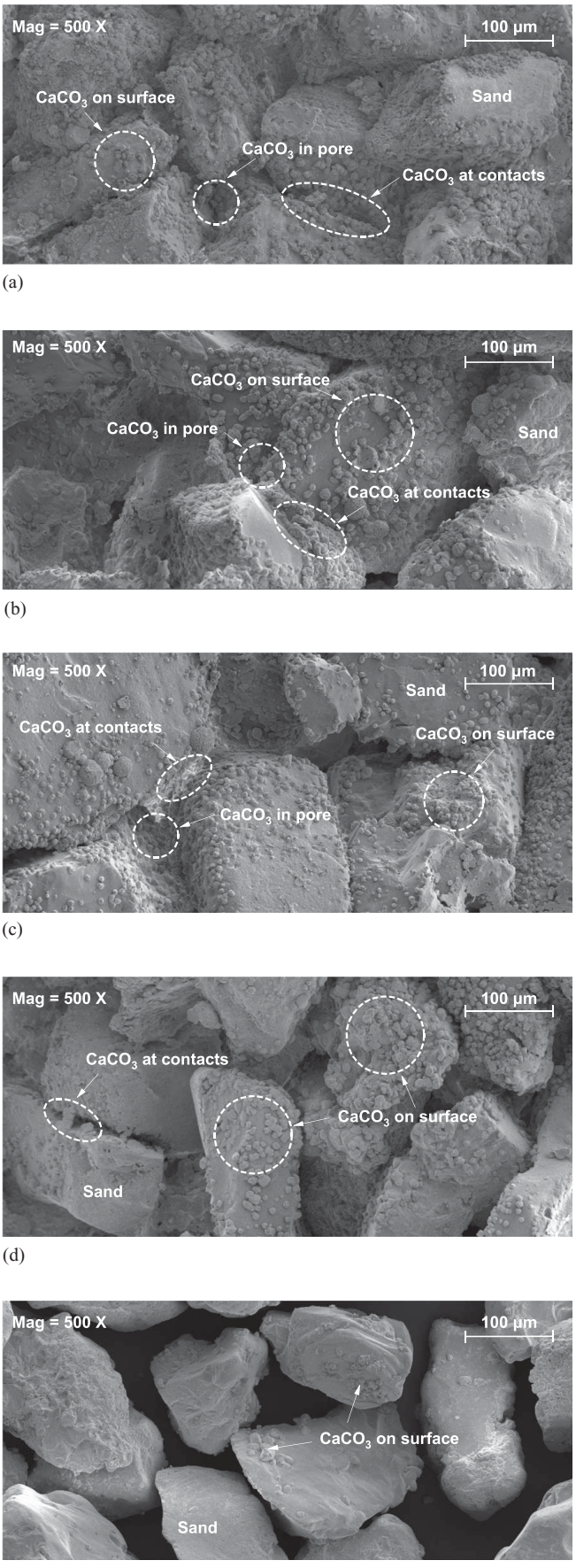

Fig. 4. SEM images of biotreated sand around the model pile: (a) $z = 0$; (b) $z = 0.1$; (c) $z = 0.2$; (d) $z = 0.3$; and (e) $z = 0.5$ m

patterns indicate that the growth of $CaCO_3$ during the MICP process can be divided into three stages. During the initial stage, the amorphous $CaCO_3$ crystals are formed and randomly attached to sand particles. In the second stage, the number and size of crystals increase due to the accumulation of calcium and carbonate ions induced by the MICP process. This leads to the formation of the bonding at the pore throat between sands particles [Figs. 4(b and c)]. During the third stage, the voids are filled by $CaCO_3$ as the crystals continuously grow, resulting in a significant decrease of pore volume as shown in Figs. 4(b and c). The sand particles were not enveloped by $CaCO_3$ crystals even at a relatively high precipitation content in the present study [Fig. 4(b)]. This may be due to the fact that the precipitation occurred in unsaturated state rather than in saturated state, in which the void fluids are more likely accumulated at the contacts of sand particles rather than coated on the surface of sand particles (Cheng et al. 2013).

Implications for Field Application

The model pile tests presented in this study verified the effectiveness of biotreatment to enhance the lateral bearing capacity of piles. In addition to the large increase in the ultimate lateral resistance, biogrouting with MICP significantly reduces the displacement at a given lateral load. The zone of precipitation reached a depth of 0.3–0.4 m at the laboratory scale and under gravity. For field application, an array of injection and extraction wells can be arranged along the desired pile length to facilitate economical and more uniform distribution of the biocementation solutions (van Paassen et al. 2010; Gomez et al. 2017).

Conclusions

This note investigates the lateral response of circular concrete piles in medium-dense sands both with and without biotreatment. Static lateral loading tests were performed on instrumented model piles embedded in untreated and biotreated sands. The spatial distribution of the precipitated $CaCO_3$ in the biotreated sand was obtained by performing acid washing on 1,800 sand samples collected after the loading test. SEM images of cemented sand samples were used to analyze the microstructure of cemented sands along the sand–pile interface. The following conclusions can be drawn:

1. Biotreatment by gravity percolation resulted in the cementation of sand and significant improvement in the lateral pile capacity. The ultimate lateral resistance of the pile within the biotreated sand is 2.6 times as large as that of the pile in the untreated sand. The increased strength of the biotreated sand resulted in a lower maximum bending moment than that for the pile in the untreated sand for a given lateral load magnitude.
2. The maximum $CaCO_3$ content was found near a depth of 0.1 m, which was also validated by results of the SEM images. The $CaCO_3$ mainly distributed within a depth of 0.2 m and the distribution is heterogeneous. The SEM images show that the $CaCO_3$ can precipitate on the surface of sand particles for increasing roughness, at the contacts of sand particles for increasing bonding strength, and in the pore void for increasing density, all of which could increase the lateral resistance of a pile.

The scope of the present study is limited to model-scale piles monotonically loaded with near-zero load eccentricity. Future studies using full-scale instrumented piles should be performed to verify the findings reported in this paper for application to large-scale conditions.

Data Availability Statement

All data, models, and algorithms generated or used during the study appear in the published article.

Acknowledgments

The authors would like to acknowledge the financial support from the National Science Foundation of China (Grant Nos. 41831282, 51922024, and 52078085). Dr. T. Matthew Evans was supported by the US National Science Foundation (Grant No. CMMI-1933355) during this work. This support is gratefully acknowledged.

Notation

The following symbols are used in this paper:

D = pile diameter;
E = Young's modulus the pile;
M = bending moment in pile;
I = area moment of inertia of the pile cross section;
$\Delta\epsilon(z)$ = difference between the tensile and compressive strain in a pile cross section at depth z; and
$\phi(z)$ = curvature.

References

Achal, V., A. Mukherjee, D. Kumari, and Q. Zhang. 2015. "Biomineralization for sustainable construction—A review of processes and applications." *Earth Sci. Rev.* 148: 1–17. https://doi.org/10.1016/j.earscirev.2015.05.008.

Al Qabany, A., K. Soga, and C. Santamarina. 2012. "Factors affecting efficiency of microbially induced calcite precipitation." *J. Geotech. Geoenviron. Eng.* 138 (8): 992–1001. https://doi.org/10.1061/(ASCE)GT.1943-5606.0000666.

Ashour, M., G. Norris, and P. Pilling. 1998. "Lateral loading of a pile in layered soil using the strain wedge model." *J. Geotech. Geoenviron. Eng.* 124 (4): 303–315. https://doi.org/10.1061/(ASCE)1090-0241(1998)124:4(303).

ASTM. 2006. *Standard practice for classification of soils for engineering purposes (Unified Soil Classification System)*. ASTM D2487-06. West Conshohocken, PA: ASTM.

ASTM. 2013. *Standard test methods for deep foundations under lateral load*. ASTM D3966/D3966M-07(2013)e1. West Conshohocken, PA: ASTM.

ASTM. 2016. *Standard test method for flexural strength of concrete (using simple beam with center-point loading)*. ASTM C293/C293M-16. West Conshohocken, PA: ASTM.

Bienen, B., J. Duhrkop, J. Grabe, M. F. Randolph, and D. J. White. 2012. "Response of piles with wings to monotonic and cyclic lateral loading in sand." *J. Geotech. Geoenviron. Eng.* 138 (3): 364–375. https://doi.org/10.1061/(ASCE)GT.1943-5606.0000592.

Chen, Y.-J., S.-W. Lin, and F. H. Kulhawy. 2011. "Evaluation of lateral interpretation criteria for rigid drilled shafts." *Can. Geotech. J.* 48 (4): 634–643. https://doi.org/10.1139/t10-094.

Cheng, L., R. Cord-Ruwisch, and M. A. Shahin. 2013. "Cementation of sand soil by microbially induced calcite precipitation at various degrees of saturation." *Can. Geotech. J.* 50 (1): 81–90. https://doi.org/10.1139/cgj-2012-0023.

DeJong, J. T., et al. 2013. "Biogeochemical processes and geotechnical applications: Progress, opportunities and challenges." *Géotechnique* 63 (4): 287–301. https://doi.org/10.1680/geot.SIP13.P.017.

Faro, V. P., N. C. Consoli, F. Schnaid, A. Thome, and L. da Silva Lopes. 2015. "Field tests on laterally loaded rigid piles in cement treated soils." *J. Geotech. Geoenviron. Eng.* 141 (6): 06015003. https://doi.org/10.1061/(ASCE)GT.1943-5606.0001296.

Feng, K., and B. M. Montoya. 2016. "Influence of confinement and cementation level on the behavior of microbial-induced calcite precipitated sands under monotonic drained loading." *J. Geotech. Geoenviron. Eng.* 142 (1): 04015057. https://doi.org/10.1061/(ASCE)GT.1943-5606.0001379.

Gomez, M. G., C. M. Anderson, C. M. R. Graddy, J. T. DeJong, D. C. Nelson, and T. R. Ginn. 2017. "Large-scale comparison of bioaugmentation and biostimulation approaches for biocementation of sands." *J. Geotech. Geoenviron. Eng.* 143 (5): 04016124. https://doi.org/10.1061/(ASCE)GT.1943-5606.0001640.

Han, F., M. Prezzi, and R. Salgado. 2017. "Energy-based solutions for non-displacement piles subjected to lateral loads." *Int. J. Geomech.* 17 (11): 04017104. https://doi.org/10.1061/(ASCE)GM.1943-5622.0001012.

Kang, X., L. Ge, and W. C. Liao. 2016. "Cement hydration-based micromechanics modeling of the time-dependent small-strain stiffness of fly ash-stabilized soils." *Int. J. Geomech.* 16 (3): 04015071. https://doi.org/10.1061/(ASCE)GM.1943-5622.0000552.

Kashizadeh, E., A. Mukherjee, and A. Tordesillas. 2021. "Experimental and numerical investigations on confined granular systems stabilized by bacterial cementation." *Int. J. Geomech.* 21 (1): 04020244. https://doi.org/10.1061/(ASCE)GM.1943-5622.0001891.

Knappett, J. A., and S. P. G. Madabhushi. 2009. "Influence of axial load on lateral pile response in liquefiable soils. Part I: Physical modelling." *Géotechnique* 59 (7): 571–581. https://doi.org/10.1680/geot.8.009.3749.

Li, Q., A. W. Stuedlein, and A. Marinucci. 2019. "Effect of casing and high-strength reinforcement on the lateral load transfer characteristics of drilled shaft foundations." *J. Geotech. Geoenviron. Eng.* 145 (9): 04019056. https://doi.org/10.1061/(ASCE)GT.1943-5606.0002116.

Lin, H., M. T. Suleiman, H. M. Jabbour, and D. G. Brown. 2018. "Bio-grouting to enhance axial pull-out response of pervious concrete ground improvement piles." *Can. Geotech. J.* 55 (1): 119–130. https://doi.org/10.1139/cgj-2016-0438.

Lin, H., M. T. Suleiman, H. M. Jabbour, D. G. Brown, and E. Kavazanjian, Jr. 2016. "Enhancing the axial compression response of pervious concrete ground improvement piles using biogrouting." *J. Geotech. Geoenviron. Eng.* 142 (10): 04016045. https://doi.org/10.1061/(ASCE)GT.1943-5606.0001515.

Liu, L., H. Liu, A. W. Stuedlein, T. M. Evans, and Y. Xiao. 2019. "Strength, stiffness, and microstructure characteristics of biocemented calcareous sand." *Can. Geotech. J.* 56 (10): 1502–1513. https://doi.org/10.1139/cgj-2018-0007.

Ma, G., X. He, X. Jiang, H. Liu, J. Chu, and Y. Xiao. 2021. "Strength and permeability of bentonite-assisted biocemented coarse sand." *Can. Geotech. J.* 58 (7): 969–981. https://doi.org/10.1139/cgj-2020-0045.

Mahawish, A., A. Bouazza, and W. P. Gates. 2019. "Unconfined compressive strength and visualization of the microstructure of coarse sand subjected to different biocementation levels." *J. Geotech. Geoenviron. Eng.* 145 (8): 04019033. https://doi.org/10.1061/(ASCE)GT.1943-5606.0002066.

Meyerhof, G. G., S. K. Mathur, and A. J. Valsangkar. 1981. "Lateral resistance and deflection of rigid walls and piles in layered soils." *Can. Geotech. J.* 18 (2): 159–170. https://doi.org/10.1139/t81-021.

Montoya, B. M., and J. T. DeJong. 2015. "Stress–strain behavior of sands cemented by microbially induced calcite precipitation." *J. Geotech. Geoenviron. Eng.* 141 (6): 04015019. https://doi.org/10.1061/(ASCE)GT.1943-5606.0001302.

Nafisi, A., B. M. Montoya, and T. M. Evans. 2020. "Shear strength envelopes of biocemented sands with varying particle size and cementation level." *J. Geotech. Geoenviron. Eng.* 146 (3): 04020002. https://doi.org/10.1061/(ASCE)GT.1943-5606.0002201.

Nasr, A. M. A. 2014. "Experimental and theoretical studies of laterally loaded finned piles in sand." *Can. Geotech. J.* 51 (4): 381–393. https://doi.org/10.1139/cgj-2013-0012.

Rahimi, M., D. Chan, and A. Nouri. 2016. "Bounding surface constitutive model for cemented sand under monotonic loading." *Int. J. Geomech.* 16 (2): 04015049. https://doi.org/10.1061/(ASCE)GM.1943-5622.0000534.

Randolph, M. F. 1981. "The response of flexible piles to lateral loading." *Géotechnique* 31 (2): 247–259. https://doi.org/10.1680/geot.1981.31.2.247.

Rollins, K. M., M. Herbst, M. Adsero, and D. Brown. 2010a. "Jet grouting and soil mixing for increased lateral pile group resistance." In *GeoFlorida 2010: Advances in Analysis, Modeling & Design*, Geotechnical Special Publication 199, edited by D. O. Fratta, A. J. Puppala, and B. Muhunthan, 1563–1572. Reston, VA: ASCE.

Rollins, K. M., J. L. Snyder, and J. M. Walsh. 2010b. "Increased lateral resistance of pile group in clay using compacted fill." In *GeoFlorida 2010: Advances in Analysis, Modeling & Design*, Geotechnical Special Publication 199, edited by D. O. Fratta, A. J. Puppala, and B. Muhunthan, 1602–1611. Reston, VA: ASCE.

San Pablo, A. C. M., et al. 2020. "Meter-scale biocementation experiments to advance process control and reduce impacts: Examining spatial control, ammonium by-product removal, and chemical reductions." *J. Geotech. Geoenviron. Eng.* 146 (11): 04020125. https://doi.org/10.1061/(ASCE)GT.1943-5606.0002377.

Stone, K. J. L., H. S. Arshi, and L. Zdravkovic. 2018. "Use of a bearing plate to enhance the lateral capacity of monopiles in sand." *J. Geotech. Geoenviron. Eng.* 144 (8): 04018051. https://doi.org/10.1061/(ASCE)GT.1943-5606.0001913.

van Paassen, L. A., R. Ghose, T. J. M. van der Linden, W. R. L. van der Star, and M. C. M. van Loosdrecht. 2010. "Quantifying biomediated ground improvement by ureolysis: Large-scale biogrout experiment." *J. Geotech. Geoenviron. Eng.* 136 (12): 1721–1728. https://doi.org/10.1061/(ASCE)GT.1943-5606.0000382.

Whiffin, V. S., L. A. van Paassen, and M. P. Harkes. 2007. "Microbial carbonate precipitation as a soil improvement technique." *Geomicrobiol. J.* 24 (5): 417–423. https://doi.org/10.1080/01490450701436505.

Xiao, P., H. Liu, A. W. Stuedlein, T. M. Evans, and Y. Xiao. 2019a. "Effect of relative density and biocementation on cyclic response of calcareous sand." *Can. Geotech. J.* 56 (12): 1849–1862. https://doi.org/10.1139/cgj-2018-0573.

Xiao, Y., H. Chen, A. W. Stuedlein, T. M. Evans, J. Chu, L. Cheng, N. Jiang, H. Lin, H. Liu, and H. M. Aboel-Naga. 2020a. "Restraint of particle breakage by biotreatment method." *J. Geotech. Geoenviron. Eng.* 146 (11): 04020123. https://doi.org/10.1061/(ASCE)GT.1943-5606.0002384.

Xiao, Y., X. He, T. M. Evans, A. W. Stuedlein, and H. Liu. 2019b. "Unconfined compressive and splitting tensile strength of basalt fiber-reinforced biocemented sand." *J. Geotech. Geoenviron. Eng.* 145 (9): 04019048. https://doi.org/10.1061/(ASCE)GT.1943-5606.0002108.

Xiao, Y., A. W. Stuedlein, Z. Pan, H. Liu, T. M. Evans, X. He, H. Lin, J. Chu, and L. A. van Paassen. 2020b. "Toe-bearing capacity of precast concrete piles through biogrouting improvement." *J. Geotech. Geoenviron. Eng.* 146 (12): 06020026. https://doi.org/10.1061/(ASCE)GT.1943-5606.0002404.

Xiao, Y., Y. Wang, C. S. Desai, X. Jiang, and H. Liu. 2019c. "Strength and deformation responses of biocemented sands using a temperature-controlled method." *Int. J. Geomech.* 19 (11): 04019120. https://doi.org/10.1061/(ASCE)GM.1943-5622.0001497.

Yang, P., E. Kavazanjian, and N. Neithalath. 2019. "Particle-scale mechanisms in undrained triaxial compression of biocemented sands: Insights from 3D DEM simulations with flexible boundary." *Int. J. Geomech.* 19 (4): 04019009. https://doi.org/10.1061/(ASCE)GM.1943-5622.0001346.

Yang, P., S. O'Donnell, N. Hamdan, E. Kavazanjian, and N. Neithalath. 2017. "3D DEM simulations of drained triaxial compression of sand strengthened using microbially induced carbonate precipitation." *Int. J. Geomech.* 17 (6): 04016143. https://doi.org/10.1061/(ASCE)GM.1943-5622.0000848.

Yu, G. M., W. M. Gong, Y. C. Liu, G. L. Dai, and M. H. Chen. 2018. "Lateral capacity of pile with grouted upper soil: Field test and numerical simulation." *Innov. Infrastruct. Solutions* 3 (1): 1–9. https://doi.org/10.1007/s41062-017-0104-5.